

# An Integrated Microtransformer System for Displacement Measurement

Matija Podhraški<sup>1</sup>, Janez Trontelj<sup>2</sup>

<sup>1</sup>Letrika Lab d.o.o, Šempeter pri Gorici, Slovenia

<sup>2</sup>Laboratory of Microelectronics, Faculty of Electrical Engineering, University of Ljubljana, Ljubljana, Slovenia

**Abstract:** The paper discusses the design and prototype evaluation of an integrated inductive microsystem used for displacement measurement, realized in the form of an ASIC. The advantage of the system is in its ability to operate without external stimulation such as a magnetic field source or an optical source used in conventional position encoders. The system comprises multiple microtransformers with corresponding analog front-end electronic circuits and is fabricated in an unmodified 350 nm CMOS process. The microtransformers consist of two concentric microcoils with their magnetic coupling dependent on the position of an external metal object, i.e. a target or a scale. The primary microtransformer winding is excited by an AC signal with a frequency of several MHz. This signal induces the secondary voltage, which has its amplitude and phase modulated by a moving metal scale. The modulation is then measured by the analog front-end as a differential output signal of two series of adjacent microtransformers geometrically shifted by a half of the scale period. The paper introduces the design and the construction of the microsystem, presents the results of the microtransformer characterization with a resolution of 100  $\mu\text{m}$ , and explains the output characteristics shape due to the asymmetry in the microtransformer pair.

**Keywords:** inductive sensor; eddy-current sensor; displacement sensor; ASIC; microtransformer

## Integriran mikrotransformatorski sistem za merjenje pomika

**Izveček:** Prispevek obravnava zasnovno in evalvacijo testnega induktivnega mikrosistema za merjenje pomika, realizirano kot namensko integrirano vezje (ASIC). Prednost sistema je možnost delovanja brez zunanega magnetnega ali optičnega vira, kot se uporabljajo pri konvencionalnih enkoderjih položaja. Sistem, ki je izdelan v nemodificiranem 350 nm CMOS procesu, obsega več mikrotransformatorjev ter ustrezen analogni vmesnik. Mikrotransformator sestavljata dve koncentrični mikrotuljavici, na magnetni sklop katerih vpliva položaj zunanega kovinskega objekta (tarče oz. merilne letve). Primarno navitje mikrotransformatorjev je vzbujano z izmeničnim signalom frekvence nekaj MHz. Ta signal inducira sekundarno napetost, ki je amplitudno in fazno modulirana s premikanjem tarče. Analogni vmesnik izmeri modulacijo kot diferencialni izhodni signal dveh zaporedij mikrotransformatorjev, ki sta geometrijsko zamaknjeni za polovico periode merilne letve. Prispevek razloži zasnovno in zgradbo mikrosistema, predstavi rezultate karakterizacije mikrosistema z ločljivostjo 100  $\mu\text{m}$ , ter pojasni obliko izhodnega signala z vidika asimetrije v paru mikrotransformatorjev.

**Ključne besede:** induktivni senzor; senzor na vrtnične tokove; senzor pomika; namensko integrirano vezje; mikrotransformator

\*Corresponding Author's e-mail: matija.podhraski@si.mahle.com

## 1 Introduction

Beside optical encoders, various types of magnetic position encoders are widely used in position sensing applications. The most common sensor mechanisms employed in these applications are based on the effect of Lorentz force onto charge carriers: Hall or magnetoresistive effect. These devices can be produced as monolithic integrated circuits using microelectronic technologies [1].

Magnetic position encoders deliver information about the linear or rotary displacement by measuring the variations in the magnetic field strength in the environment. The spatially variable, position-dependent time-stationary magnetic field is commonly generated using a magnetized scale or a fixed magnet. The availability and cost, as well as environmentally questionable production [2] of rare earth elements, which are currently the key magnetic materials, can present an issue for the

position encoder industry. Additionally, conventional optical encoders also require an external light source (e.g. a LED) [1].

Since the industry is in constant search for reliable, precise, robust, dimension- and cost-effective position encoders, research in unconventional sensor principles is strongly encouraged. It is our belief that encoders fabricated in the form of an ASIC, without requiring additional components and/or costly wafer postprocessing for their fabrication, will play an important role in the future. The presented issues of conventional sensors, as well as expected trends in position sensor industry, have led us into research of the possibilities of ASIC implementation of the inductive position sensing, which is also common in industrial applications [1].

The main difference of inductive sensing concept in comparison to magnetic encoders is in the fact that a time-variable magnetic field of a certain frequency is employed instead of a stationary magnetic field.

For detecting the presence of the object (i.e. without precise determination of an object position), two major types of inductive proximity sensors are in widespread use:

1. A dual-coil structure; the first coil, connected to an AC source, induces the voltage in the second coil. If a conductive object (the target) is moved into the vicinity of the coils, eddy currents are induced in the conductor, generating a magnetic field opposing the field of the first coil. The voltage in the secondary coil is thus reduced due to the eddy current energy loss in the target [1,3].
2. An oscillatory type, where a coil (or in some cases, a transformer) is used as the inductive part of a resonant circuit. When the target is approached, the inductance of the coil changes, resulting in the change of the oscillator resonant frequency [1,4].

Another benefit of inductive sensors beside the aforementioned lack of need for permanent magnetic elements, is their insensitivity to dust, which presents a strong advantage in an industrial environment in comparison to the optical sensors [3].

## 2 Microsystem design

### 2.1 Differential operation of a microtransformer

The paper addresses the topic of integrating an inductive position sensing microsystem on a single silicon die. The discussed system employs a concept of opera-

tion similar to a linear variable differential transformer (LVDT) [5], and also to an eddy current sensor [6–8]. The sensor is scaled to a dimension of a typical integrated circuit (several square millimeters). The design of the microtransformer arrangement used in the sensor is shown in Figure 1.

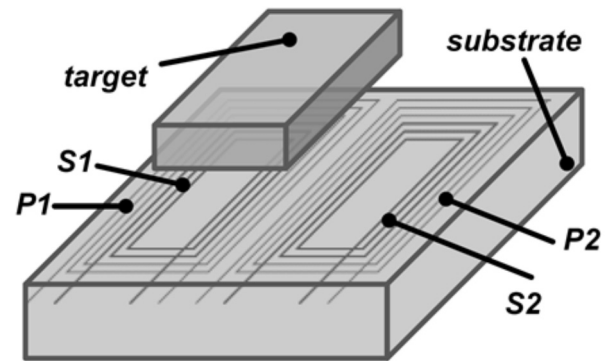


**Figure 1:** The structure of the discussed sensor, comprising two microtransformers, P denoting a primary winding and S denoting a secondary winding.

Figure 2 explains the differential operation of the microtransformer. When the full half-period of the ferromagnetic scale is positioned centrally over the first microtransformer, the coupling between the primary and the secondary is the strongest for this microtransformer. Contrarily, the coupling is then the weakest for the second microtransformer as the void half-period is positioned over it. The differential voltage  $V_{diff}$  of the microtransformer pair is obtained by subtracting the secondary voltages of microtransformers  $V_a$  and  $V_b$  [8]. In the described situation,  $V_{diff}$  amplitude is maximal. As the scale moves, the outputs change periodically. It should be noted that for a conductive (non-ferromagnetic) scale, the operation is adversary [7], shifting the signals for 180°; when a microtransformer is completely covered with a part of metal, its induced voltage is minimal due to eddy-current dissipation of the field energy in the scale.

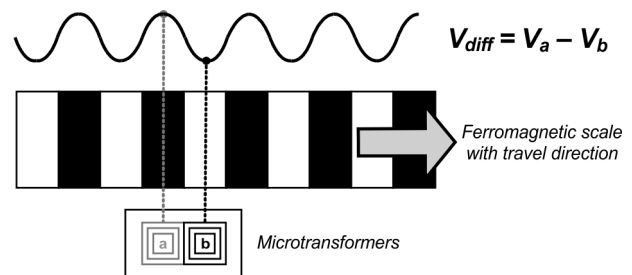


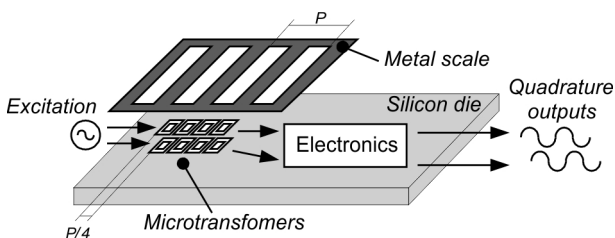
**Figure 2:** The differential operation of the microtransformer.

Using the presented differential principle, the signals which are common to both microtransformers in a

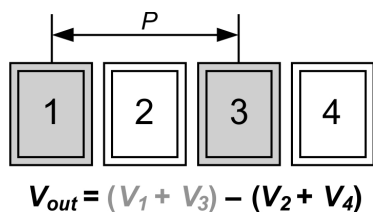
pair, e.g. electromagnetic interference and, most importantly, the capacitively transferred voltage between the primary and secondary winding, are subtracted [7]. This capacitively transferred voltage can easily exceed the inductively coupled voltage [6]. The previously described subtraction of the two signals can be carried out using either opposite connection of the secondary windings or a differential amplifier. The second option is used in the presented design, since it proves being less demanding to ensure the symmetry of the signal paths from the winding outputs to the amplifier [8].

2.2 *Microsystem construction*

The design of the microsystem is presented in Figure 3 (a). It consists of a silicon die comprising the microtransformers along with analog front-end electronics for the generation of the differential signal. The microtransformers are fabricated using standard CMOS technology metal layers. The total layer count is four. The typical external dimensions of the microtransformer primary and secondary windings are 755 by 500 μm and 576 by 314 μm, respectively. Therefore the adequate scale period  $P$  is 1 mm. Each winding of a microtransformer has 45 turns: three layers with 15 turns per layer are used, while one metal layer is used for routing the interconnections [8].



a)



b)

**Figure 3:** a) A block representation of the presented microsystem with a metal scale of period  $P$  and quadrature output signals. b) The summation scheme of the presented microsystem comprising four microtransformers per channel.

The number of the microtransformers can be increased, thus improving the signal-to-noise ratio by summing the output voltages of coils with same position inside a distinct scale period, while the primary windings are connected in parallel, thus being synchronously excit-

ed [8]. The summation scheme used in the presented system comprising four microcoils per channel is presented in Figure 3 b).

As presented in Figure 3 a), the sensor comprises two channels shifted for a quarter of the scale period, thus yielding quadrature output signals [6].

The quadrature principle is commonly employed by position encoders (e.g. optical encoders [9] and Hall sensors [10]), relying on two sensor elements with their position shifted by a half of the primary coil width (i.e.  $\frac{1}{4}$  of the scale period). Quadrature signals are important since observing their phase shift allows the determination of the movement direction. Moreover, if the signals have a sinusoidal shape, the arctangent function of their amplitude ratio

$$x = \arctan \left( \frac{\sin x}{\cos x} \right) \tag{1}$$

provides the linear information about the position  $x$  inside one scale period [10].

The schematic of the integrated circuit with the realized analog front-end is shown in Figure 4. The circuit comprises operational amplifiers in the first stage (generating signals  $y_1$  and  $y_2$ ) with a DC gain of 10 and a transconductance amplifier (OTA) used for the generation of the differential signal  $d$  (followed by voltage buffer, which is not shown in the figure). The reason for the use of the transconductance amplifier is in its lack of need of feedback circuit, since its gain and thus the output voltage is mainly determined by the amplifier load (not shown) and its transconductance [11]. As the modulation of the signals is relatively weak (e.g. 5 % of amplitude, which, for example, results in target period full voltage swing of 250 μV at a microtransformer

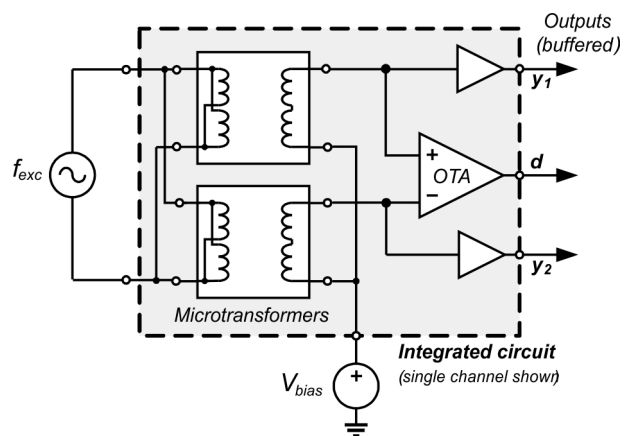


**Figure 4:** The block diagram of the integrated circuit, also presenting the summation scheme of the microtransformers.

output of 5 mV), the input impedance of an amplifier should remain the same for the positive ( $y_1$ ) and the negative signal ( $y_2$ ). The gain of the implemented OTA is in the range of 100-300, falling with the rise of the excitation signal frequency.

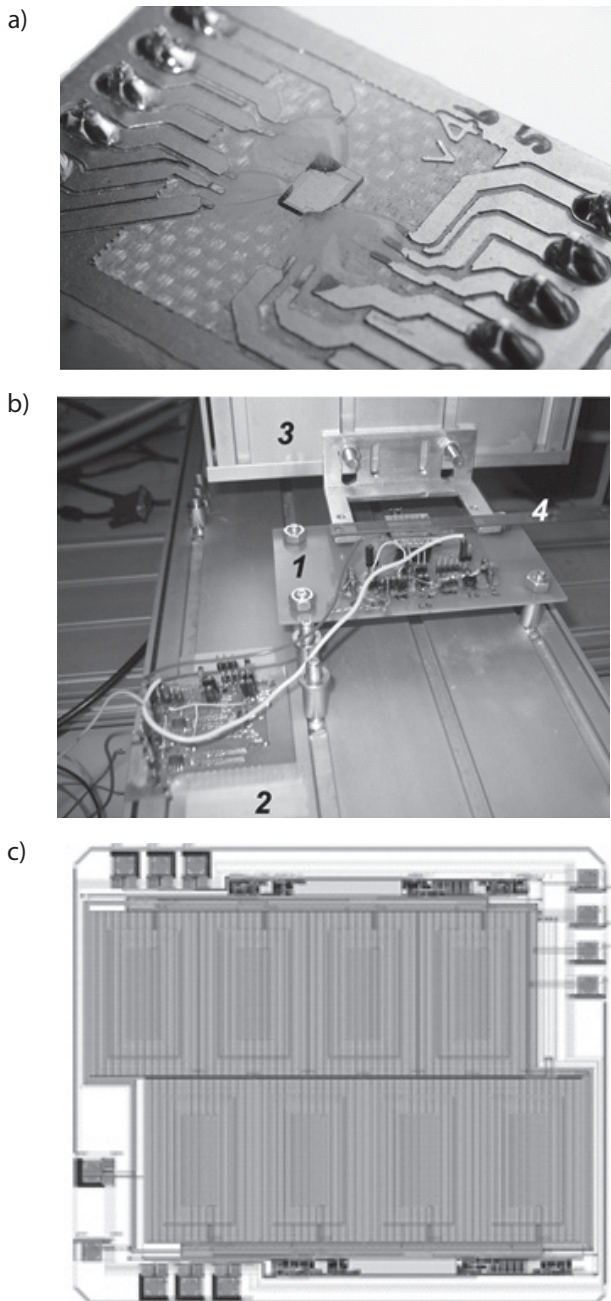


**Figure 5:** (a) A close photograph of the test IC on its prototype PCB board. (b) A photograph of the evaluation system comprising a two-channel IC on a mounting board (1), an external processing circuit (2), motorized mechanical manipulator (3) and the ferromagnetic target scale (4). (c) The layout of the IC, comprising eight microtransformers and the described integrated electronics.

The fabricated IC is shown mounted on a evaluation board in Figure 5 a). The complete evaluation system comprising the board is shown in Figure 5 b), while the layout of the integrated circuit is shown in Figure 5 c).

### 3 System evaluation

The performance of the presented version of the microsystem was evaluated using a system presented schematically in Figure 6, while its photograph is shown in Figure 5 b).

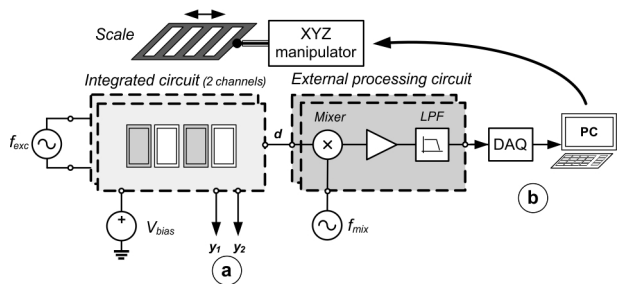


**Figure 6:** The microsystem evaluation configuration. The measurement setup is shown for a single channel (the IC comprises two quadrature channels).

The summed output signal of two odd-positioned microtransformers (i.e. signal  $y_1$  in Figure 6), amplified by a non-inverting on-chip operational amplifier with a DC gain of 10) was measured first. This measurement is represented by "a" in Figure 6. The results are graphically presented in Figure 7. The transfer characteristic of the microsystem was recorded using a network analyzer HP 3577A. The amplitude and phase characteristics (in relation to the excitation signal of 1 V) were recorded for uncovered IC ("No target"), for silicone steel (transformer core lamination sheet material of 0.35 mm thickness) and aluminum targets (a relatively large block of 0.5 mm approximate thickness). A large piece of material (i.e. at least ten times the IC area) was used as the target, completely covering the IC. The shape of the curves after 3 MHz is unrelated to the target, as the integrated amplifier transfer function starts to prevail, its pole strongly reducing the amplifier gain at higher frequencies [11]. The measurement data at 2 MHz are given in Table 1.

The sensor performance was then evaluated with a moving ferromagnetic scale (transformer core lamination sheet material of 0.35 mm thickness), perforated with void areas of 0.5 mm width (measurement "b" in Figure 6). In this evaluation, the differential sensor outputs were downmixed to a low-frequency signal which was then acquired by a computer. A photograph of the complete evaluation system is shown in Figure 5 b).

**Table 1:** The measured network analyzer data at 2 MHz; see Figure 7. The modulation and the phase difference are calculated relative to the “No target” situation.

Material	Amplitude [mV]	Phase [°]	Modulation M [%]	Phase difference [°]
No target	21.8	-169.3	-	-
Aluminum	19.6	-173.5	-10.1	-4.2
Steel	29.6	-164.3	35.8	5.0

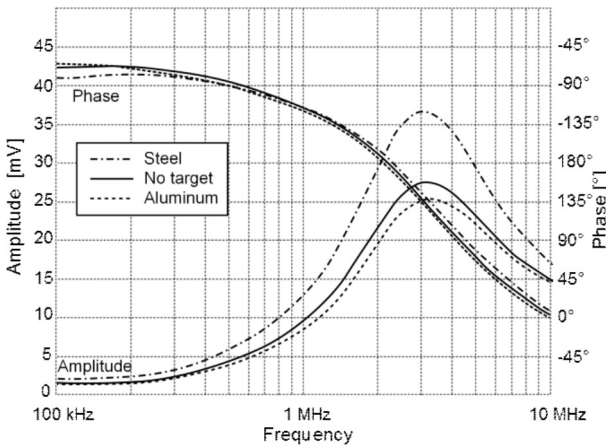


**Figure 7:** Network analyzer measurements of different target effects performed on a prototype microsystem.

In the reported evaluation, the excitation frequency  $f_{exc}$  was 1.8 MHz and the excitation signal was sinusoidal with  $5 V_{pp}$ . The mixing frequency  $f_{mix}$  was 1.801 MHz, thus resulting in the output intermediate frequency (IF) of 1 kHz. This output IF signal was acquired using a 12-bit Data Acquisition (DAQ) interface. A computer (running MATLAB) was used to determine the peak-to-peak value of the voltage at each position of the scale, which is graphically presented in Figure 8. The scale position was also controlled by the computer through a motorized manipulator with a PC interface. The positioning step was 100  $\mu m$ . Figure 8 presents the evaluation results for three samples of the IC prototype. Two quadrature channels were measured. In both described measurements, the distance between the silicon die surface and the scale was approximately 200-300  $\mu m$ . This distance is determined by the height of bonding wires connecting the IC to its prototype board (Figure 5 (a)), which are covered with a gel protective coating, as they need to be mechanically protected from tearing.

A rectified signal shape with an offset, as well as large differences between the two channels on a same IC and also between the samples are evident from Figure 8, especially in the second measurement channel. To understand the sources of this signal shape, the modeling of the scale modulation was carried out, which is presented in the next chapter.

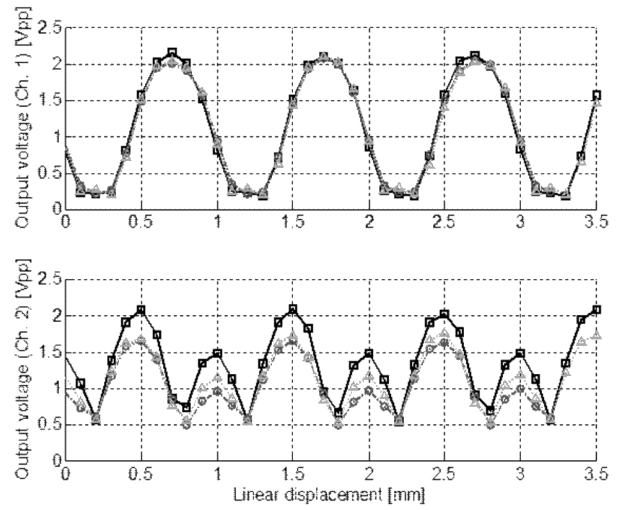


**Figure 8:** The recorded dependence between the linear displacement and the output voltage for three IC samples and for the two channels on each IC. Linear interpolation between the points is used.

#### 4 The modeling of the scale modulation

The effect of the target is modeled by amplitude modulation of the excitation signal (also named the carrier signal) with a frequency  $f_{exc}$ . A frequency 100 times lower than the carrier frequency is chosen as the modulation frequency. In a physical system, this frequency ratio could be much higher – the modulation signal can be also thought of as a static (DC) multiplication signal, when the system is not in the movement. Actually, the modulation signal’s periodicity and the actual shape are associated to the physical structure and the position of the scale. In this analysis, the sinusoidal modulation is transformed into the time domain as an arbitrary frequency signal for modeling purposes.

Two counterphase modulated signals  $y_1$  and  $y_2$  with amplitudes  $A_1$  and  $A_2$  (representing the positive and the negative microtransformer outputs), are used as the representation of the microtransformer output signals.

$$y_1 = A_1 (1 + m_1 \sin(2\pi f_m t + \phi_{m1})) \sin(2\pi f_c t + \phi_{c1}) \quad (2)$$

$$y_2 = A_2 (1 - m_2 \sin(2\pi f_m t + \phi_{m2})) \sin(2\pi f_c t + \phi_{c2}) \quad (3)$$

The modulation indices  $m_1$  and  $m_2$  correspond to the intensity of the modulation. The phase shift angles  $\phi_{xx}$  of the carrier and modulation signals are also included in the equations. Then, the output signal is obtained as the difference between the two microtransformer output signals:

$$d = y_1 - y_2 \tag{4}$$

It is necessary to remark that the amplifier also produces gain, while this is not significant to this analysis.

Supposing all phase angles  $\varphi_{xx}$  in Equations (2) and (3) are zero, and the modulation factor is the same for the both signals ( $m_1 = m_2 = m$ ), Equation (4) yields through the use of prosthaphaeresis formulae:

$$d = (A_1 - A_2) \sin(2\pi f_c t) + m \frac{A_1 + A_2}{2} (\cos(2\pi(f_c - f_m)t) - \cos(2\pi(f_c + f_m)t)) \tag{5}$$

The shape of the difference signal  $d$  for several illustrative combinations of the carrier signal amplitude asymmetries ( $A_1 \neq A_2$ ) and modulation factors is shown in Figure 9. In the bottom part of the figure, it can be seen that the asymmetry has less effect on the signal shape if the modulation index is high. Contrarily, if the modulation index is low and asymmetry is strong enough (examples in the upper right quarter of the figure), the

signal never reduces to zero. The shape of the curve starts to resemble a harmonic signal.

The analysis was carried out using sinusoidal modulation functions, since the shape of the measured signals (Figure 8) resembled a (rectified) sinusoidal. However it has been proven valid also for other shapes of modulation functions, e.g. triangular. It is also necessary to remark that the asymmetry of the modulation indices ( $m_1 \neq m_2$ ) has a similar effect on the shape of the difference signal as the amplitude asymmetry ( $A_1 \neq A_2$ ).

The measurements on the fabricated prototypes (presented in Figure 7 and Table 1) show that the phase of the signals  $y_1$  and  $y_2$  also changes in the presence of the target. Therefore, in reality, a combination of amplitude and phase modulation is present, introducing distortions in the envelope of the difference signal, which is desired to have a shape as close to sinusoidal as possible. The reason for this is in the method for the calculation of the position using the arctangent function (Equation 1). Evidently, expression (5) would be considerably more complex if it also accounted for the phase differences and additional real effects, such as non-symmetric target scale geometry and especially the scale misalignment, which would introduce the modulation factor asymmetry.

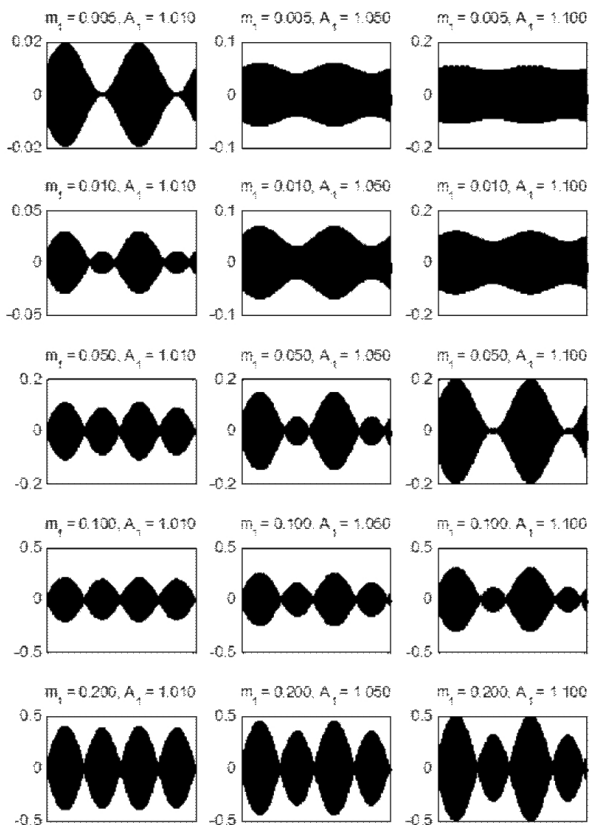


**Figure 9:** Examples of differential signal  $d$  shapes with different asymmetries and modulation factors.  $A_1$  and  $m_1$  are varied, while  $A_2$  and  $m_2$  are set to 1.

## 5 Conclusion

The paper first presented the basic concept of inductive sensors for position measurement and some disadvantages of conventional position encoders which can be alleviated using the proposed integrated sensor concept. The presented design has the sensing elements (i.e. the microtransformers) integrated along with the analog front-end, using the identical metal layers as the CMOS circuits, which differs from the previous work [12,13]. The system design and operation were presented and supported with measurements on fabricated prototypes. The measurements have shown the feasibility of the design, confirming the appropriateness of the proposed sensor design for an ASIC realization. The expected modulation characteristics for both ferromagnetic and conductive targets were experimentally demonstrated using solid targets covering the entire microsystem.

Further evaluation using a measurement scale has shown the need for the investigation of the modulation effects of the difference signal. The signal has a shape of a pulsating curve, which is heavily dependent on the asymmetry between the two signals subtracted in the process of differential signal generation. The

signal needs further processing to be converted into a smooth sinusoidal signal, which will allow the determination of the linear position from the quadrature signals using arctangent interpolation, as described in [8].

## 6 Acknowledgments

The authors thank to Boštjan Fink and Daniele Bertocchi for preparing the layout of prototype integrated circuits and to the remaining staff of the LMFE Laboratory and Letrika Lab d.o.o. for fruitful discussions, support and pleasant working atmosphere.

## 7 References

1. Fraden, J. *Handbook of Modern Sensors: Physics, Designs, and Applications*; Springer Science & Business Media, 2010.
2. Alonso, E.; Sherman, A. M.; Wallington, T. J.; Everson, M. P.; Field, F. R.; Roth, R.; Kirchain, R. E. Evaluating Rare Earth Element Availability: A Case with Revolutionary Demand from Clean Technologies. *Environ. Sci. Technol.* 2012, *46*, 3406–3414.
3. Fleming, A. J. A review of nanometer resolution position sensors: Operation and performance. *Sens. Actuators Phys.* 2013, *190*, 106–126.
4. Weiwen, L.; Hui, Z.; Hongli, Q. Research on novel grating eddy-current absolute-position sensor. *IEEE Trans. Instrum. Meas.* 2009, *58*, 3678–3683.
5. Spiezia, G.; Losito, R.; Martino, M.; Masi, A.; Pierno, A. Automatic Test Bench for Measurement of Magnetic Interference on LVDTs. *IEEE Trans. Instrum. Meas.* 2011, *60*, 1802–1810.
6. Podhraški, M.; Trontelj, J. Design and evaluation of a microcoil proximity sensing microsystem. *Conf. 2015 Proc. 51<sup>th</sup> Int. Conf. Microelectron. Devices Mater. Workshop Terahertz Microw. Syst. Sept. 23 - Sept. 25 2015 Bled Slov.* 2015, *2015*, 95–99.
7. Bergqvist, J. W.; Coulon, Y. de; Lambilly, H. de Device for detecting position and movement by using magnetic field variation, US6043644 A, 2000.
8. Podhraški, M.; Trontelj, J. A Differential Monolithically Integrated Inductive Linear Displacement Measurement Microsystem. *Sensors* 2016, *16*, 384.
9. Rozman, J.; Pletersek, A. Linear Optical Encoder System With Sinusoidal Signal Distortion Below 60 dB. *IEEE Trans. Instrum. Meas.* 2010, *59*, 1544–1549.
10. Hoang, H. V.; Jeon, J. W. Signal compensation and extraction of high resolution position for sinusoidal magnetic encoders. In *International Conference on Control, Automation and Systems, 2007. ICCAS '07*; 2007; pp. 1368–1373.
11. Razavi, B. *Design of Analog CMOS Integrated Circuits*; McGraw-Hill Education: Boston, MA, 2000.
12. Passeraub, P. A.; Besse, P.-A.; Bayadroun, A.; Hediger, S.; Bernasconi, E.; Popovic, R. S. First integrated inductive proximity sensor with on-chip CMOS readout circuit and electrodeposited 1 mm flat coil. *Sens. Actuators Phys.* 1999, *76*, 273–278.
13. Kejlik, P.; Kluser, C.; Bischofberger, R.; Popovic, R. S. A low-cost inductive proximity sensor for industrial applications. *Sens. Actuators Phys.* 2004, *110*, 93–97.

Arrived: 31. 12. 2015

Accepted: 26. 04. 2016